Industrial Chemistry & Materials

ROYAL SOCIETY OF CHEMISTRY

PAPER

View Article Online
View Journal | View Issue

Cite this: *Ind. Chem. Mater.*, 2024, **2**, 141

Synergistic functionalization of poly(*p*-terphenyl isatin) anion exchange membrane with quaternary ammonium and piperidine cations for fuel cells†

Yiman Gu,[a] Yanchao Zhang,[a] Zhe Wang, *[b] Di Liu,[b] Yan Wang,[a] Tianming Dong,[a] Song Wang,[a] Zhanyu Li,[a] Jingyi Wu[a] and Yijia Lei[a]

Received 13th July 2023,
Accepted 8th September 2023

DOI: 10.1039/d3im00077j

rsc.li/icm

Research on anion exchange membrane fuel cells (AEMFCs) mainly focuses on the membrane module, and improving its performance has always been the focus of researchers. To create high-performance anion exchange membranes (AEMs), a series of side chain type AEMs were prepared by introducing different proportions of side chains containing anisotropic poly cations with relatively stable piperidinium ring cations and side quaternary ammonium cations as cation groups, using poly(*p*-terphenyl isatin) (PTI), a main chain polymer without aryl ether bonds. The dense surface of the PTI-N-*n* series membranes is shown by SEM images; TEM images show that the ion domains are clearly distributed in the membrane, so a continuous ion transport channel is constructed. PTI-N-100 has the highest hydroxide conductivity at 80 °C, reaching 96.83 mS cm^{-1} due to multiple transport sites. The PTI-N-100 membrane has a peak power density of 180 mW cm^{-2} based on the highest ionic conductivity. Therefore, we believe that the introduction of multi-cations contributes to the performance of anion exchange membranes.

Keywords: Multi-cation; Ether-free polymer; Alkaline resistance; Microphase separation.

1 Introduction

At present, there are fewer and fewer non-renewable resources on earth, and the atmosphere is deteriorating. Based on the inherent requirements of sustainable development, clean energy has become a major trend in international energy development. In the past few decades, the excessive use of non-renewable energy sources such as peat, natural gas, oil, and coal has produced waste gases containing a lot of harmful substances, which has led to increasingly serious air pollution. Clean energy can eliminate the emissions of harmful substances such as carbon dioxide and sulfur dioxide, thus reducing air pollution. Moreover, using clean energy can greatly reduce the damage to the atmosphere and contribute to human health and development. The application of fuel cells is an effective way to resolve the lack of oil resources.[1] Many research institutes in the world automotive community are already carrying out extensive research activities targeting fuel cells in areas such as advances in zero and ultra-low emission vehicle power. Proton exchange membrane fuel cells (PEMFCs)[2] have good characteristics and are considered by many research institutes and car manufacturers to be the obvious choice for fuel cells for automobiles. Unlike PEMFCs, anion exchange membrane fuel cells (AEMFCs) are superior in that: (1) the cathode has high redox capacity under alkaline conditions, so it is unnecessary to use noble metal catalyst;[3] (2) the alkaline medium in the AEMFCs replaces the alkaline medium in the PEMFCs, thus reducing the influence of acid corrosion.[4] As a strategic high-tech industry, membrane materials[5] are a strategic requirement for carbon neutrality targets. Not only that, but ensuring the storage of membranes in strong alkaline conditions is the most critical problem in the development of AEMFCs, so polymer formation strategies that focus primarily on high chemical stability, mechanical stability, and ionic conductivity are an effective means of promising to unlock the next phase of anion exchange membranes (AEMs). This will trigger a new wave of innovation leading to the accelerated development of highly efficient fuel cells for sustainable development.

The AEM is constructed of cationic groups and a polymer skeleton. Commonly, some polymers that have been commercially used as anion exchange membrane scaffolds are poly(ether ether ketone) (PEEK),[6–8] poly(phenylene oxide) (PPO),[9–13] and poly(ether sulfone) (PSF).[14–17] Their

[a] *College of Chemical Engineering, Changchun University of Technology, Changchun, 130012, China*
[b] *School of Chemistry and Life Science, Changchun University of Technology, Changchun, 130012, China. E-mail: wzccut@126.com*

† Electronic supplementary information (ESI) available. See DOI: https://doi.org/10.1039/d3im00077j

structures all contain aryl ether bonds that are vulnerable to attack by OH^- or –OH radicals. The presence of aryl ether bonds may lead to the breakage of the main chain and thus accelerate the degradation of the membrane. Therefore, the use of ether-free bonded polymers in anion exchange membranes has received attention from researchers, such as polyolefins,[18,19] polybenzimidazoles,[20] poly(aryl piperidinium),[21–23] and crown ether polymers.[24,25] Li *et al.*[26] reported a series of polyolefin copolymer-based AEMs at 80 °C for 20 days in 10 M NaOH solution, which exhibited excellent alkali stability; Zhu *et al.*[27] studied the anion exchange membrane based on polybenzimidazole as the skeleton through the polycondensation reaction, which showed a high alkaline stability at 80 °C in 1 M NaOH for more than 1000 hours; Wang *et al.*[28] fabricated AEMs containing a macrocyclic host–guest structure with dynamic self-protection. The membranes achieved a hydroxide conductivity of 114 mS cm^{-1} at 80 °C. The membranes achieved 93% ion retention after immersion in 5 M KOH at 80 °C for 1000 h; Zhu *et al.*[29] prepared poly(aryl piperidinium) anion exchange membranes with nitrogen heterocyclic cations. The PBP-BOP-ASU (8%) membrane showed the highest ionic conductivity at 80 °C (117.43 mS cm^{-1}). When it was kept in a 2 M NaOH solution at 80 °C for 1400 hours, it showed excellent alkali stability. However, Zhu *et al.*[30] prepared an anion-exchange membrane with poly(terphenyl isatin piperidinium) as the main chain to further balance the "trade-off" problem. Due to the crosslinked structure and the high alkali resistance of the ether-free polymer backbone, the membranes maintained ≥85% hydroxide conductivity after 1600 h of treatment in a 3 M NaOH solution at 80 °C. The membrane was found to be highly resistant to alkaline attack. As a result, the alkali stability of AEMs made of ether-free polymers is outstanding.

In addition, common cations are linked to the main chain in the form of benzyl groups. However, under strong base conditions, benzyl groups are unstable and vulnerable to attack by hydroxide ions, which can be degraded by the S_N2 reaction.[31] To solve this problem, on the one hand, imidazoles,[32,33] quaternary phosphonium[34,35] and metal cations[36–38] have been found; on the other hand, many teams have focused on the design aspects of molecular structures, such as the introduction of cross-linking reagents.[39] Such proposed cross-linking strategies are a successful way to enhance the mechanical characteristics of membranes and reduce gas permeation. However, after the introduction of cross-linking agents without conductive sites, the alkali resistance is improved, but the ionic conductivity is sacrificed accordingly. In order to solve this problem, the researchers put forward cationic groups far away from the main chain to promote micro-phase separation.[40–42] Build ion transport channels by using hydrophilic cationic groups to separate from the hydrophobic polymer backbone to construct a more pronounced micro-phase separation structure. This enhances the base resistance stability of the anion exchange membrane while improving conduction. However, in order to improve conduction more effectively, methods of establishing multiple transmission points have been proposed.[43]

In the current work, ether-free bonded poly(*p*-terphenyl isatin) (PTI) was prepared as the backbone of an anion exchange membrane by introducing different polycationic side chains in different proportions through a simple and nontoxic super acid catalytic reaction, and an anion exchange membrane with good ionic conductivity was developed. A series of tests will be carried out to investigate the effect of quaternary ammonium cations and piperidine cations acting together as side chains on membrane properties such as hydrophilicity, ionic conductivity, and base stability. In this study, the molecular structure of AEMs is schematically shown in Scheme 1.

2 Results and discussion

2.1 Synthesis and molecular structure characterization

The ^{1}H NMR spectrum of PTI-N-*n* is an important basis for testing whether the product was successfully prepared. The synthesis path of PTI-N-*n* is shown in Scheme 2. Fig. 1a shows the ^{1}H NMR characteristics of each of 4-ClPq and 3-N-4-ClPq. Fig. 1b shows the ^{1}H NMR spectrum of PTI, which was successfully synthesized from hydroquinone and indirubin by a metal-free "click reaction" under the catalysis of superacid. The single peak at 10.87 ppm is the N–H proton signal on the indigo, and the signal at 7.02–7.78 ppm comes from the phenyl proton on the main chain of *p*-terphenyl and the isatin benzene ring, which proves that the main chain is successfully synthesized. Fig. 2 takes PTI-N-80 as an example, and compares the spectra of PTI and PTI-N-80. From the Fig. 2, the peak of the indigo N–H proton signal at 10.87 ppm in PTI-N-80 is significantly weakened, indicating that some of isatin N–H reaction. The signal peak at 3.01 ppm belongs to the cationic group, and the signal peaks at 3.83 ppm is attributed to methylene protons on the connected isatin and quaternary ammonium groups, respectively. The

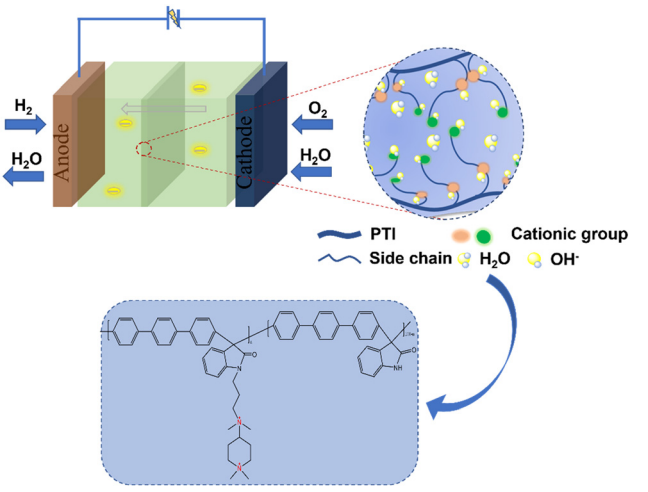

Scheme 1 Schematic diagram of the molecular structure of AEMs with multi-cation side alkyl chains.

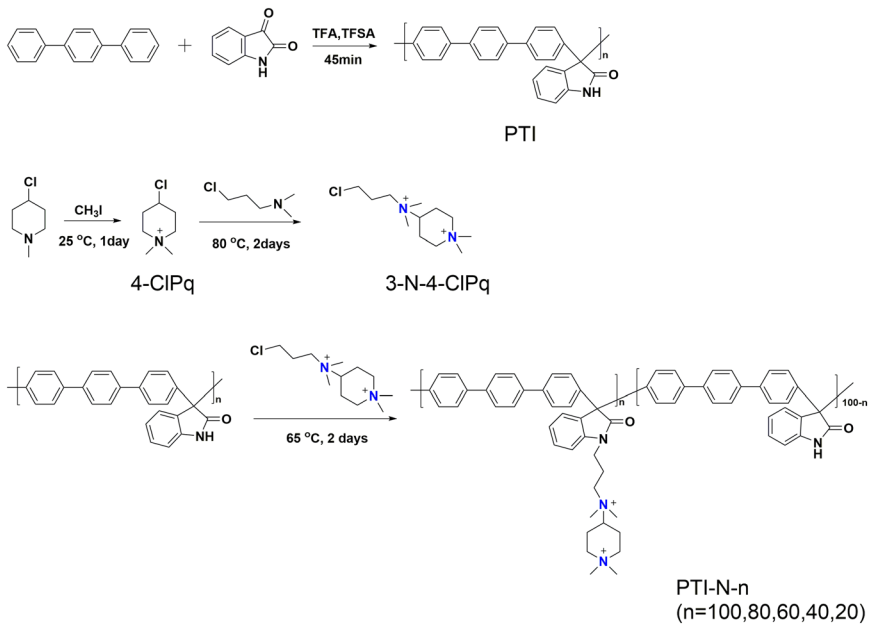

Scheme 2 Synthesis route of PTI-N-*n*.

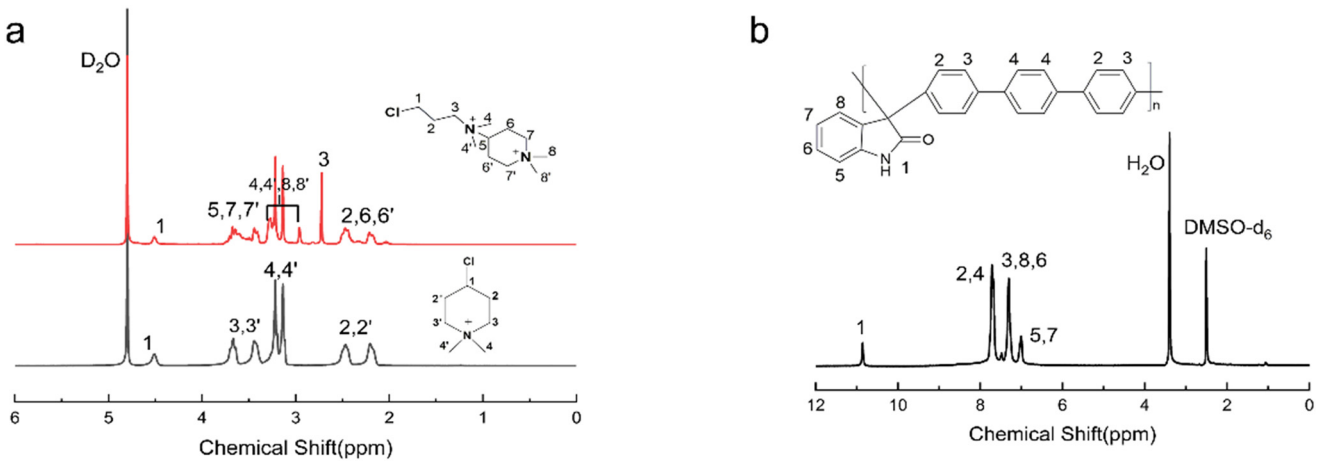

Fig. 1 ^{1}H NMR spectra of (a) 4-ClPq and 3-N-4-ClPq; (b) poly(*p*-terphenyl isatin).

signal peaks of methylene and alkyl chain protons in the piperidine ring on 4-ClPq were found at 1–2 ppm, which proved that PTI-N-80 was successfully synthesized by comparison.

Besides, the FT-IR spectra is an important way to prove the successful synthesis of the products. PTI-N-100 was taken as an example, as shown in Fig. 3, we tested the infrared spectra of PTI and PTI-N-100. The bending vibration peak of –NH at 3381 cm^{-1} and the stretching vibration peak of –NH at 1662 cm^{-1} appeared in the infrared image of PTI, but disappear in the infrared image of PTI-N-100, indicating that the reaction of –NH group on the main chain has been completed. In the IR image of PTI-N-100, a characteristic absorption peak of $–CH_2–$ on the alkyl side chain appears at 1354 cm^{-1}, which is not found on PTI. In short, it can be proved that PTI-N-100 was successfully synthesized.

2.2 Micromorphology

In Fig. 4, the images of the surface and cross section of PTI-N-100 membrane were recorded by SEM. The membrane surface is smooth and compact without holes, preventing fuel leakage. The thickness of the PTI-N-100 is 22 μm, which is appropriate for fuel cells. As shown in Fig. 4a and b, after repeated immersion and washing in deionized water, the PTI-N-100 membrane showed no obvious defects or cracks in both pictures of the membrane, which indicated that the grafted functionalized monomer successfully existed in the membrane without being dissolved in deionized water, on the other hand, it also showed the dense structure of the membranes.

The micro-phase separation structure of AEMs is closely related to the performance of the membrane, and TEM is

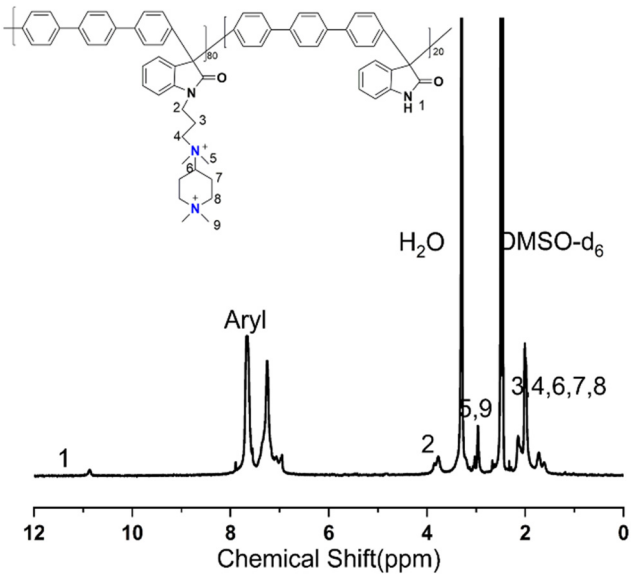

Fig. 2 ^{1}H NMR spectra of PTI-N-80.

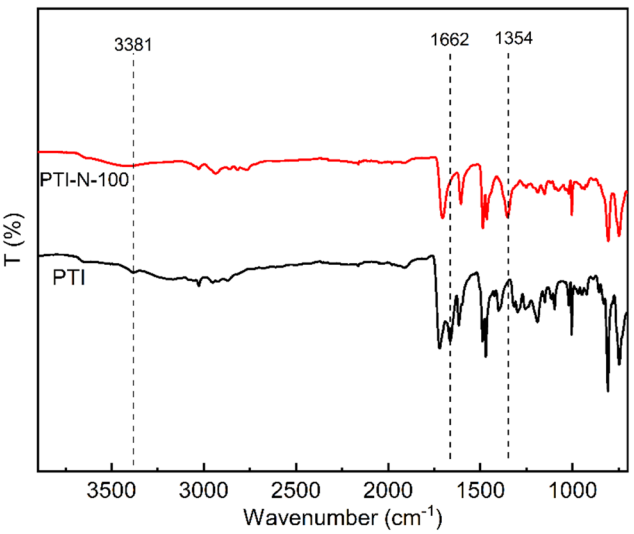

Fig. 3 FT-IR spectra of PTI and PTI-N-100.

one means of observing the structure within the membrane. The TEM images of PTI-N-20, PTI-N-60, and PTI-N-100 in OH^- form are shown in Fig. 4c–e, in which the phase separation structure with obviously curved bands can be clearly observed. The light and dark phases each represent the hydrophobic and hydrophilic phases of the AEM. Therefore, as shown in Fig. 4, with the increase of the proportion of the hydrophilic side chain, the range of the dark areas increases accordingly. The comparison shows that the PTI-N-100 has the most remarkable microphase separation, so it has the highest ionic conductivity, which follows the same pattern as the ion conductivity test results.

We further demonstrated the microscopic phase separation morphology of PTI-N-*n* series membranes by AFM. The dark area represents the hydrophilic domain in the membrane, while the light area indicates the hydrophobic domain of the main chain in the membrane. As can be seen from Fig. 5a and b, PTI-N-100 presents a more obvious microphase separation structure than PTI-N-20. This is the same as the TEM test results, so the increase in the proportion of side chains can bring about obvious micro-morphological changes.

In addition, we conducted a SAXS test (Fig. S1†). However, as can be seen in the figure, no scattering peaks were found in the interval. The reason for this result may be due to the high rigidity of the poly(*p*-terphenyl isatin) main chain, which is consistent with the previous literature reports on poly(arylene) AEMs.[30,44,45]

2.3 Ion exchange capacity (IEC), water uptake (WU), swelling rate (SR)

The ion exchange capacity (IEC) represents the content of cationic groups through which anions are transported in the AEM. Generally speaking, with the increase of cationic groups, IEC tends to rise. In addition, the rise of temperature will lead to the instability of water uptake as well as swelling ratio, so it is necessary to ensure an appropriate increase in water uptake as well as swelling ratio and ionic conductivity.[46] This shows that the measured IEC is close to the theoretical IEC and PTI-N-100 has the highest IEC value, which is attributable to the fact that the more side chains effectively increase the number of anion transport sites.[47] Accordingly, a higher IEC leads to a higher concentration of hydrophilic cationic groups, and an increase of hydrophilic areas leads to a corresponding increase in water uptake.[48] Similar to other isatin-based membranes, the WU of PTI shows low dependence on temperature.[49–51] However, PTI-N-*n* series membranes all have a suitable swelling ratio, all of which are lower than 45%, showing good dimensional stability. Meanwhile, as the temperature increases, the WU and SR are positively related to the temperature. In order to further characterize the water uptake of the PTI-N-*n*, as shown in Fig. 6c, the water contact angle of PTI-N-100 is 62.9°, while the water contact angle of PTI-N-20 is 75.7°, which is consistent with the increasing trend of WU, showing good hydrophilicity of the prepared membrane.[52–54] This is consistent with the consequence of the microphase separation morphology shown in transmission tests (Table 1).

2.4 Hydroxide ion conductivity (σ)

The ionic conductivity is an important index for determining the performance of AEMs, which represents the strength of the anion exchange membrane's ability to transport ions. As shown in Fig. 6d, we have tested the ionic conductivity of AEM with different proportions of heterologous polycationic side chains. According to Fig. 6d, PTI-N-*n* series membranes are positively correlated with temperature. The reason is that the increase of temperature accelerates the molecular movement inside the membranes, increases the OH^- mobility and improves the conductivity of PTI-N-*n*. The hydroxide conductivity of PTI-N-80 is 41.76 mS cm^{-1} at 30 °C as well as

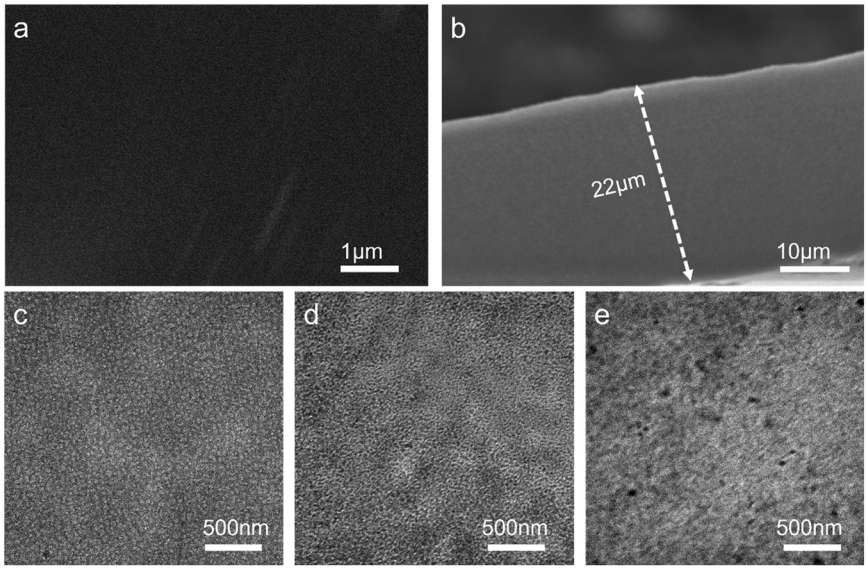

Fig. 4 (a) Surface and (b) cross-sectional SEM images of the PTI-N-100 membrane; TEM images of (c) PTI-N-20, (d) PTI-N-60 and (e) PTI-N-100 membranes, respectively.

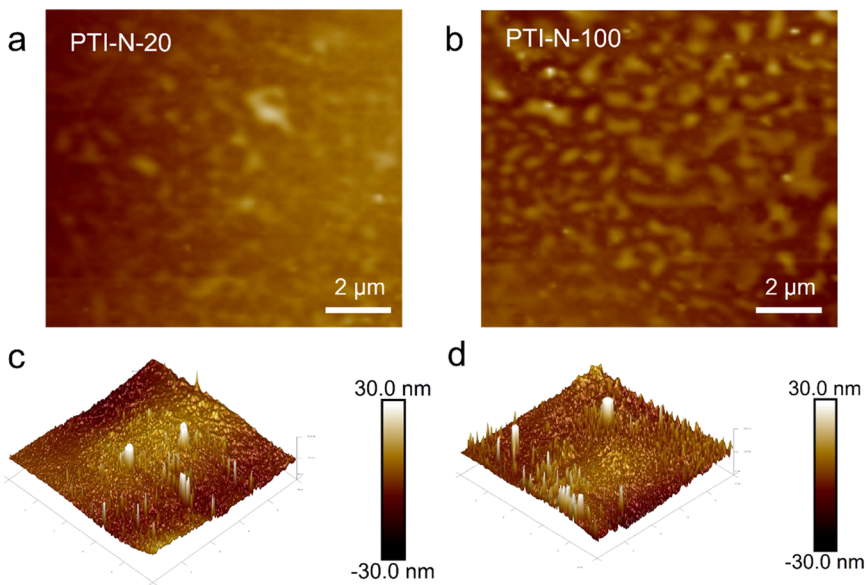

Fig. 5 AFM phase images and 3D height topography of PTI-N-20 and PTI-N-100.

80.92 mS cm^{-1} at 80 °C. With the increase of temperature, the ionic conductivity shows an upward trend. In addition, the side chain content increased gradually, and the ionic conductivity also presented a trend of increasing. Due to the influence of multiple transmission sites, the PTI-N-100 membrane presented the highest ionic conductivity at 80 °C, which was 96.83 mS cm^{-1}. The formation of microphase separation structure in PTI-N-100 membrane is effectively improved by high cation concentration, which makes it easier to form the aggregation of hydrophilic regions and thus improves ionic conductivity. This is because many cations are introduced, more OH^- transport sites are provided and multiple ion transport channels are established. The whole series of AEMs has good ionic conductivity. As shown in Fig. 6e, the Arrhenius plot of the fitted membrane was used to calculate its activation energy from the slope of the straight line. We found that the PIT-N-100 membrane has the lowest activation energy, which proves that it requires less ion migration energy and is more prone to ion migration. This is consistent with the pattern of OH^- ion conductivity.

2.5 Thermal stability

The anion exchange membranes prepared must not only have good dimensional stability, but also maintain good stability under certain temperature environments. For AEMs, good thermal stability can be effective in avoiding performance losses of alkaline fuel cells during operation. As shown in

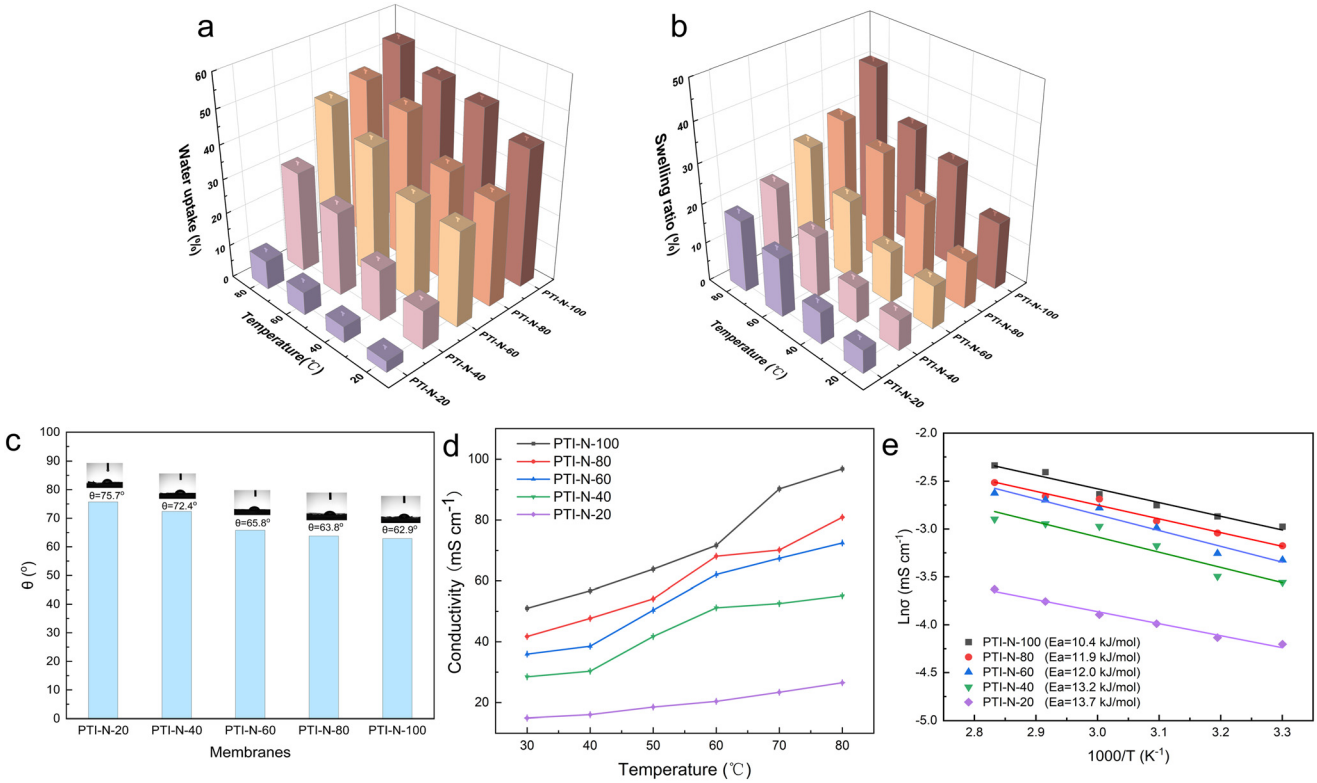

Fig. 6 (a) Water uptake and (b) swelling ratio of the PTI-N-*n* membranes; (c) the water contact angle; (d) hydroxide conductivity and (e) Arrhenius plots of PTI-N-*n* membranes.

Table 1 IEC, WU, SR, and σ of PTI-N-*n*

	IEC (mmol g^{-1})		WU (%)		SR (%)		σ (mS cm^{-1})	
Samples	Theoretical value	Measured value	20 °C	80 °C	20 °C	80 °C	30 °C	80 °C
PTI-N-100	3.38	3.16	41.27	54.10	17.13	41.05	51	96.83
PTI-N-80	2.93	2.74	31.58	48.00	12.16	31.18	41.76	80.92
PTI-N-60	2.41	2.07	28.57	45.00	11.02	28.30	35.95	72.44
PTI-N-40	1.77	1.62	11.54	30.00	7.71	22.05	28.47	55.14
PTI-N-20	0.99	0.97	3.42	8.70	5.93	18.32	14.96	26.52

Fig. 7a, the weight loss before 150 °C is due to the evaporation of traces water and solvent remaining in the AEM. Evaporation of combined water and some solvents in the membrane will lead to a slight decrease in the thermogravimetric curve. The second stage of degradation at 220 °C to 350 °C, which is mainly due to the degradation of the cations. The loss of the cationic groups at this temperature is enough for the application of AEMFCs. In the third stage, degradation of the primary chain of the polymer occurred above 550 °C, which indicates that the poly(*p*-terphenyl isatin) had good high temperature resistance. According to TGA curve, a series of AEMs prepared by experiment have good thermal stability, as well as after high temperature TGA analysis, the quality of PTI-N-*n* series membranes is retained at least 40%, the results show that this series of AEM are enough to meet the requirements of AEMFCs. It also demonstrates the good thermal stability of poly(*p*-terphenyl isatin) as an AEM backbone, which has a long-term application prospect in alkaline temperature fuel cell applications.

2.6 Mechanical properties

During the process of fuel cell assembly and testing, there are some harsh conditions which require that the anion exchange membranes have enough mechanical properties to withstand the test. At 100% relative humidity, the mechanical properties of PTI-N-*n* membranes were tested as shown in Fig. 7b. The tensile strengths of the membranes ranged from 20.13–59.53 MPa, as well as the elongations at break were all in the range of 5–17.64%. The pure PTI membrane shows excellent dimensional stability, and the tensile strength is 59.53 MPa. However, the tensile strength of the membranes will decrease with the increase of the content of side chain branching. As the content of branched chains increases, the unit volume of the molecular chain increases, increasing the

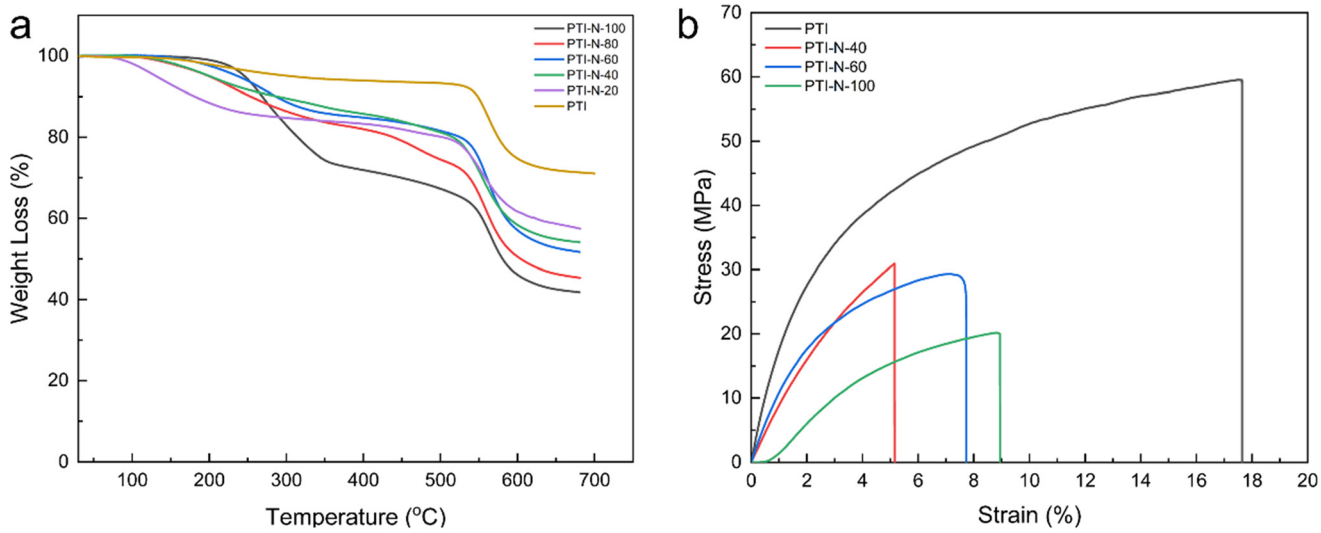

Fig. 7 The graphs of (a) TGA curves of PTI-N-*n* membranes; (b) stress–strain curves of PTI-N-*n* membranes.

water uptake of the AEMs, which weakens the interaction of the polymer backbone and leads to a decrease in tensile strength.[55–57] All PTI-N-*n* membranes showed suitable tensile strength, which proves the good prospect of poly(*p*-terphenyl isatin) as the skeleton of anion exchange membrane (Table 2).

2.7 Alkaline stability

The alkali-resistant stability of AEM is an important factor to check whether the fuel cell can operate stably, and it is also the main reason to restrict the development of fuel cell. The attack of nucleophilic OH^- on cations and main chains is the main cause of degradation of AEM. The retention rate of ionic conductivity for PTI-N-100 and PTI-N-20 are shown in Fig. 8a, in which AEM was continuously immersed in a 2 M KOH at 80 °C for nearly 800 hours. During this period, the ionic conductivity of the membrane was tested at several time intervals, and the data was used to continuously monitor the overall downward trend of ionic conductivity. The monitoring data (a) showed that PTI-N-100 had good alkali stability, and after 792 hours, PTI-N-100 still maintained its initial ionic conductivity of 65.46%. This is due to the special geometric conformation of the piperidine ring cation in the side chain. Through the elimination of transition state and the geometric constraint of substitution, OH^- corrosion can be effectively reduced, thus improving the alkali resistance.[58] In addition, the selection of the main chain without ether bond reduces the probability of OH^- attacking the ether bond of the main chain, and the alkali resistance is further improved.[44]

Fig. 8b shows the ^1H NMR comparison diagram of PTI-N-100 before and after the alkali stability test. From the comparison diagram, it is easy to see that the proton characteristic peaks on the benzene ring of poly(*p*-terphenyl isatin) have not obviously moved or changed, which proves the excellent alkali stability of the poly(*p*-terphenyl isatin). The possible causes of membrane degradation derived from the NMR are (1) nucleophilic substitution of the QA functional group by OH^- attack, leading to the formation of alkyl alcohols,[59] a degradation pathway that is identified by the appearance of the signal at 4.5 ppm and 0.86 ppm. (2) Hofmann elimination reaction of β-H of the piperidinium due to attack by OH^-, identified by the signal peaks at 5.01 ppm and 5.68 ppm in the nuclear magnetogram.[60] As can be seen from the figure, the main degradation is carried out by the above two ways. It is worth mentioning that the alkali resistance of quaternary ammonium cations was poor in previous studies,[61] and we expected that the introduction of piperidone with special geometrical conformations and ether-free bonded backbones would improve the alkali resistance of the membranes. From the comparison of the results, this synergistic structural design did improve the alkali resistance.

Table 2 Mechanical properties of PTI-N-*n* membranes

Samples	Thickness (mm)	Tensile strength (MPa)	Elongation at break (%)
PTI	25	59.53	17.64
PTI-N-40	23	30.93	5.06
PTI-N-60	26	29.36	7.73
PTI-N-100	22	20.18	8.94

2.8 Single H_2/O_2 fuel cell performance

Fuel cell performance is a necessary indicator to test the commercialization and viability of AEMs. To some extent, it reflects their practical application. For the tests, we used PTI-N-100 to assemble the membrane electrodes. The polarization curve of PTI-N-100 is shown in Fig. 9. Fuel cells assembled from PTI-N-100 membrane have 0.86 V open-

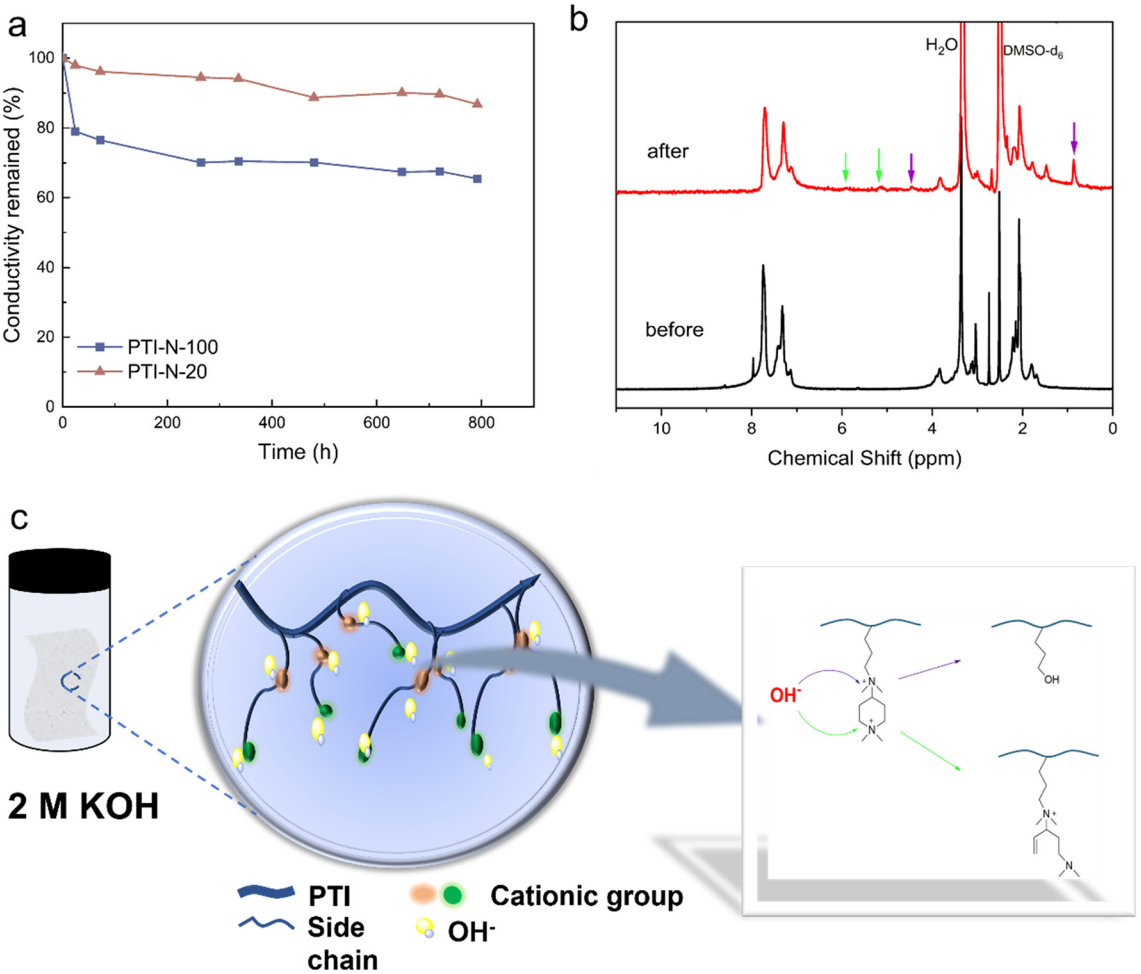

Fig. 8 (a) Curves of ionic conductivity retention *versus* immersion time of the membranes in 2 M KOH at 80 °C; (b) ^{1}H NMR of PTI-N-100 membranes after alkali stability testing and (c) schematic diagram of degradation mechanism.

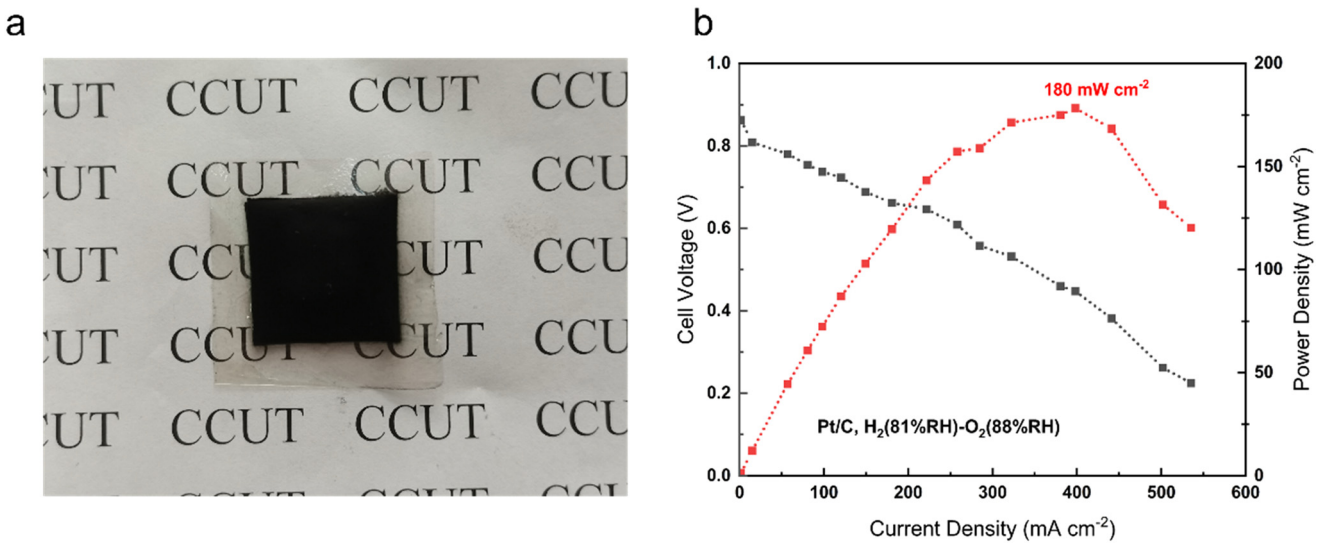

Fig. 9 (a) PTI-N-100 membrane electrode physical photo; (b) single-cell performance of AEMFCs with PTI-N-100 membranes at a cell temperature of 80 °C.

circuit voltage and 180 mW cm^{-2} peak power density, and there is no back pressure (Fig. 10).[62–66]

3 Conclusion

In summary, PTI polymers functionalized with different ratios of heterogeneous multi-cation side chains were designed. The preparation for developing excellent AEMs with good conductivity and long-term stability is made by molecular structure design. PTI-N-100 has an appropriate swelling rate of 41.05% at 80 °C, but it has high IEC, water absorption, good hydrophilicity and obvious microphase separation structure. The reason is that the dense cation groups in the membrane are beneficial to the transmission of anions. The introduction of multi-cations provides more OH^- transport sites and constructs multiple ion transport channels, thus making the ionic conductivity of AEM better. This series of PTI-N-*n* membranes reached a maximum of 96.83 mS cm^{-1} at 80 °C. Its wet mechanical strength is good, which is greater than 20 MPa. The thermal performance test shows that the main chain has higher thermal decomposition temperatures, which can reach 550 °C respectively. The hydroxide conductivity of PTI-N-100 remained 65.46% after nearly 800 h of alkali stability testing in 2 M KOH by AEMs, showing good long-term alkali stability. It shows that the highly rigid polymer skeleton has made outstanding contributions to improving the performance of AEM. The construction of an ether-free backbone reduces the chance that OH^- attacks the backbone. At the same time, the combination of two different half-life cations ensures the alkali stability of the AEM. The test results show that the good comprehensive properties of PTI anion exchange membrane functionalized by quaternary ammonium and piperidine cations can be compared with most AEMs reported so far. PTI-N-100 membrane have 0.86 V open-circuit voltage and 180 mW cm^{-2} peak power density. This means that different molecular structure design schemes have an important impact on improving the performance of anion exchange membranes.

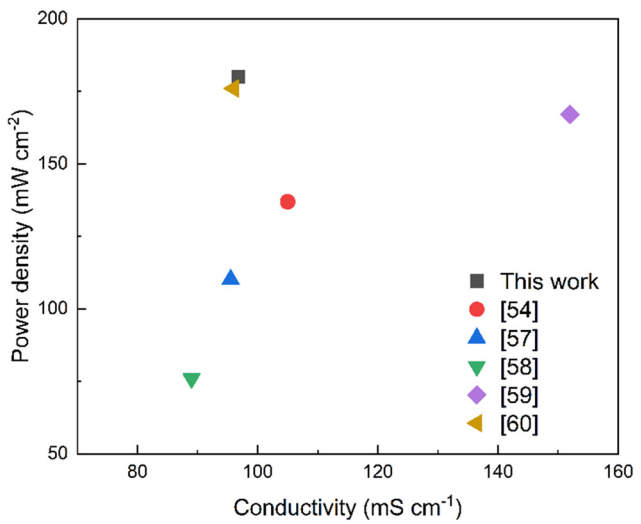

Fig. 10 Plot of power density and conductivity of PTI-N-100 with those of AEMs in other reports.

4 Experimental section

4.1 Materials

4-Chloro-1-methylpiperidine (98%), *p*-terphenyl (99%), isatin (98%), 3-chloro-1-(*N*,*N*-dimethyl) propylamine (98%), K_2CO_3 (99%), trifluoroacetic acid (TFA, 99%), iodomethane (99%), trifluoromethanesulfonic acid (TFSA, 98%) were purchased from Aladdin. The dichloromethane (99.5%) and dimethyl sulfoxide (DMSO) were purchased from Tianjin Fine Chemical Co., Ltd.

4.2 Synthesis of polymers

Poly(*p*-terphenyl isatin) (PTI) was synthesized by super acid-catalyzed stepwise polymerization. In a three-necked flask, *p*-terphenyl (1.0 g, 4.3 mmol) and isatin (0.69 g, 4 mmol) were dissolved in dichloromethane at 0 °C. TFSA (3.3 mL) and TFA (3.3 mL) were slowly dropped into the flask and mixed for 45 minutes. When the color of the mixed solution turns red-brown, it slowly precipitates in methanol to form a slightly yellowed solid. The polymer was cut into small pieces, boiled with an ethanol and deionized water solution, and dried at 40 °C for 24 hours.

4.2.1 Synthesis of 4-ClPq. 4-Chloro-1-methylpiperidine (1.2934 g, 9.68 mmol) was dissolved in ethyl acetate (50 mL) and stirred at 25 °C for 5 minutes. Methyl iodide (4.8458 g, 34.14 mmol) was added under magnetic stirring, and the mixture was stirred for 24 hours at 25 °C.

4.2.2 Synthesis of 3-N-4-ClPq. 3-Chloro-1-(*N*,*N*-dimethyl) propylamine (1 g, 0.009 mol) was dissolved in 20 mL of DMSO and stirred for 5 minutes. Then, 4-ClPq (2 g, 0.0099 mol) was added dropwise to the solution and reacted at 80 °C for 48 hours.

4.2.3 Synthesis of PTI-N-*n*. The specific synthesis steps for PTI-N-100 are: purge the three-necked flask several times with N_2. PTI (1 g, 0.0035 mol) was completely dissolved in 20 mL DMSO, then 3-N-4-ClPq (2.7 g, 0.007 mol) and K_2CO_3 (0.96 g, 0.007 mol) were added at 65 °C and reacted for 48 h. The unreacted K_2CO_3 was filtered out, and the solution was poured into ethyl acetate and dried at 40 °C to obtain a yellowish solid. Due to the adjustment of the molar ratio of PTI main chain and 3-N-4-ClPq, PTI-N-*n* (*n* = 80, 60, 40, 20) is obtained.

4.2.4 Membrane preparation. PTI-N-*n* was dissolved in DMSO (2 wt%) to prepare AEM, the solution was evenly spread on the glass board, and the glass board was dried in an oven at 80 °C for 24 h.

4.3 Characterization and measurements

4.3.1 Structure characterization. Molecular structures of PTI and PTI-N-*n* (*n* = 100, 80, 60, 40, 20) were confirmed by nuclear magnetic resonance hydrogen spectroscopy (^1H

NMR). The ^{1}H NMR spectra were obtained at 500 MHz by a Bruker NMR spectrometer. FTIR was measured by the Nicolet Avatar-360 spectrometer, and the scanning range was from 700 to 4000 cm^{-1}.

4.3.2 Performance characterization. Scanning electron microscopy (SEM) was used to observe the external morphology of the membrane. SEM tests were carried out on a JEOL-7610F. AEM was washed in deionized water, then dried under vacuum, and the images were observed at a 15 kV accelerated voltage. TEM was analyzed with an 80 kV accelerating voltage on the JEOL-2000 EX. Before measurement, samples were prepared by soaking the product in a 0.5 M KI solution for 2 days, then drying it overnight in vacuum, dissolving it in dimethyl sulfoxide, and fishing out the membrane with a copper mesh.

4.3.3 Ion exchange capacity (IEC), water uptake (WU), swelling ratio (SR). The IEC value is calculated by molar titration of the number of effective functional groups in the membrane. The IEC of AEM is determined by the reverse titration method. First, immerse the AEM samples in the form of OH^- in the standard solution of V_1 mL, 0.01 mol L^{-1} (C_1) HCl for ion exchange. After that, the membranes were removed and washed with deionized water to remove the residual salt on the surface, and the membrane samples were dried to a constant weight, and the dry weight m_{dry} was recorded. Finally, adding phenolphthalein as indicator, titrating with 0.01 mol L^{-1} (C_2) NaOH standard solution and recording the volume of alkali consumed (V_2). The IEC formula is as follows:

$$\mathrm{IEC} = \frac{C_1V_1 - C_2V_2}{m_{dry}}$$

The water uptake test of AEM is to dry the membrane sample in an oven at 80 °C and dry it to the constant weight of m_{dry}. The film samples were immersed in deionized water at 20 °C, 40 °C, 60 °C and 80 °C respectively for 24 h. After 24 h, the membrane samples were removed, and the surface moisture of the membrane samples was quickly dried with filter paper and weighed to obtain m_{wet}. WU was calculated as follows:

$$\mathrm{WU} = \frac{m_{wet} - m_{dry}}{m_{dry}} \times 100\%$$

The swelling rate test of AEM is roughly the same as the water absorption test: after drying the membrane sample, the membrane thickness was measured to d_{dry}. At different temperatures, the membrane thickness was measured by soaking for 24 h and drying the surface water to obtain d_{wet}. SR was calculated as follows:

$$\mathrm{SR} = \frac{d_{wet} - d_{dry}}{d_{dry}} \times 100\%$$

4.3.4 Ion conductivity. Ion conductivity is measured from 0.1 Hz to 105 Hz by using the four-probe impedance method (AC). AEM is installed in a PTFE mold, and the distance between the reference electrodes is 1 cm. Fully hydrated samples with a size of 1 × 5 cm were immersed in a water bath for testing. A (cm^2) is the cross-sectional area of the membrane and L (cm) is the distance between the mold electrodes. Hydroxide conductivity (σ, mS cm^{-1}) was calculated as follows:

$$\sigma = \frac{L}{R \times A}$$

4.3.5 Thermal stability. The thermal stability test of AEM was completed on PerkinElmer Pyris thermogravimetric analyzer. The test process is in N_2. Heat from 30 °C to 800 °C at a heating rate of 10 °C min^{-1}. The thermal stability of the test sample was tested in the form of OH^-.

4.3.6 Mechanical properties. The mechanical strength of AEM was tested by Shimadzu AGS-X electronic universal testing machine (100 N, Japan). The membrane was cut into 5 mm wide and 30 mm long membrane samples and tested at a stretching rate of 1 mm min^{-1}.

4.3.7 Alkaline stability. The AEM samples were immersed in 2 mol L^{-1} KOH solution at 80 °C for a period of time. After washing the alkaline solution on the surface of the membrane with ultra-pure water, the ionic conductivity data were tested and the alkali resistance curve was obtained.

4.3.8 Fuel cell performance. First, the Pt/C catalyst was coated on the surface of the carbon papers, and the loading content of the catalyst for both two electrodes was 0.5 mg cm^{-2}. Then the membrane was immersed in 1 M NaOH aqueous solution at ambient temperature for 24 h and sandwiched in the middle of carbon papers to fabricate membrane electrode assembles (MEAs). Finally, the performance of the single H_2/O_2 fuel cell was tested at 75 °C at the anode and 77 °C at the cathode with both H_2 and O_2 fluxes of 150 mL min^{-1} and no back pressure.

Conflicts of interest

The authors declare no conflict of interest.

Acknowledgements

The authors gratefully acknowledge the financial support of this work by Natural Science Foundation of China (grant no 22075031), Jilin Provincial Science & Technology Department (grant no 20220201105GX).

References

1 Y. Ligen, H. Vrubel and H. Girault, Energy efficient hydrogen drying and purification for fuel cell vehicles, *Int. J. Hydrogen Energy*, 2020, **45**, 10639–10647.
2 S. Zhang, W. Chen, S. Fan, F. Cui, S. Liu, G. He and X. Wu, Selection of competitive adsorption additives to relieve

product inhibition of maleic acid hydrogenation in proton exchange membrane flow cell reactor: A molecular dynamics simulation, *Int. J. Hydrogen Energy*, 2022, **47**, 34616–34627.

3 Y. Duan, Y. Pang, B. Liu, L. Wu, X. Hu, Q. Li and C. Zhao, Synergistic utilization of a CeO_2-Anchored bifunctionalized metal–organic framework in a polymer nanocomposite toward achieving high power density and durability of PEMFC, *ACS Sustainable Chem. Eng.*, 2023, **11**, 5270–5283.

4 W. E. Mustain, M. Chatenet, M. Page and Y. S. Kim, Durability challenges of anion exchange membrane fuel cells, *Energy Environ. Sci.*, 2020, **13**, 2805–2838.

5 P. Zuo, C. Ye, Z. Jiao, J. Luo, J. Fang, U. S. Schubert, N. B. McKeown, T. L. Liu, Z. Yang and T. Xu, Near-frictionless ion transport within triazine framework membranes, *Nature*, 2023, **617**, 299–305.

6 J. Han, H. Peng, J. Pan, L. Wei, G. Li, C. Chen, L. Xiao, J. Lu and L. Zhuang, Highly stable alkaline polymer electrolyte based on a poly (ether ether ketone) backbone, *ACS Appl. Mater. Interfaces*, 2013, **5**, 13405–13411.

7 X. Du, H. Zhang, M. Li and Z. Wang, Improved conductivity and stability of anion exchange membranes by introducing steric hindrance and crosslinked structure, *Int. J. Hydrogen Energy*, 2019, **44**, 22129–22136.

8 M. Kumari, J. C. Douglin and D. R. Dekel, Crosslinked quaternary phosphonium-functionalized poly (ether ether ketone) polymer-based anion-exchange membranes, *J. Membr. Sci.*, 2021, **626**, 119167.

9 J. Hou, X. Wang, Y. Liu, Q. Ge, Z. Yang, L. Wu and T. Xu, Wittig reaction constructed an alkaline stable anion exchange membrane, *J. Membr. Sci.*, 2016, **518**, 282–288.

10 B. Lin, F. Xu, F. Chu, Y. Ren, J. Ding and F. Yan, Bis-imidazolium based poly (phenylene oxide) anion exchange membranes for fuel cells: The effect of cross-linking, *J. Mater. Chem. A*, 2019, **7**, 13275–13283.

11 C. Lin, Y. Zhuo, A. Lai, Q. Zhang, A. Zhu, M. Ye and Q. Liu, Side-chain-type anion exchange membranes bearing pendent imidazolium-functionalized poly (phenylene oxide) for fuel cells, *J. Membr. Sci.*, 2016, **513**, 206–216.

12 L. Liu, W. Ma, J. Zhang, Z. Liu, D. Chu, R. Shao, S. Chen, X. Chu and N. Li, The design and synthesis of a long-side-chain-type anion exchange membrane with a hydrophilic spacer for alkaline fuel cells, *J. Membr. Sci.*, 2023, **678**, 121663.

13 J. Xue, X. Liu, J. Zhang, Y. Yin and M. D. Guiver, Poly (phenylene oxide)s incorporating N-spirocyclic quaternary ammonium cation/cation strings for anion exchange membranes, *J. Membr. Sci.*, 2020, **595**, 117507.

14 J. Choi, M.-H. Kim, J. Y. Han, J. E. Chae, W. H. Lee, Y. M. Lee, S. Y. Lee, J. H. Jang, J. Y. Kim, D. Henkensmeier, S. J. Yoo, Y.-E. Sung and H.-J. Kim, Application of spirobiindane-based microporous poly (ether sulfone)s as polymeric binder on solid alkaline exchange membrane fuel cells, *J. Membr. Sci.*, 2018, **568**, 67–75.

15 X. Wang, C. Lin, Q. Zhang, A. Zhu and Q. Liu, Anion exchange membranes from hydroxyl-bearing poly (ether sulfone)s with flexible spacers via ring-opening grafting for fuel cells, *Int. J. Hydrogen Energy*, 2017, **42**, 19044–19055.

16 D. Liu, M. Xu, M. Fang, J. Chen and L. Wang, Branched comb-shaped poly (arylene ether sulfone)s containing flexible alkyl imidazolium side chains as anion exchange membranes, *J. Mater. Chem. A*, 2018, **6**, 10879–10890.

17 S. Li, H. Zhang, K. Wang, F. Yang, Y. Han, Y. Sun, J. Pang and Z. Jiang, Anion conductive piperidinium based poly (ether sulfone): Synthesis, properties and cell performance, *J. Membr. Sci.*, 2020, **594**, 117471.

18 C. R. Peltier, W. You, D. F. Volcanjk, Q. Li, A. J. Macbeth, H. D. Abruña and G. W. Coates, Quaternary ammonium-functionalized polyethylene-based anion exchange membranes: Balancing performance and stability, *ACS Energy Lett.*, 2023, **8**, 2365–2372.

19 L. Liu, Y. Deng, W. Zhang, J. Zhang, W. Ma, L. Li, X. Zhang and N. Li, Highly alkali-stable polyolefin-based anion exchange membrane enabled by N-cyclic quaternary ammoniums for alkaline fuel cells, *J. Membr. Sci.*, 2023, **672**, 121441.

20 M. Guo, T. Ban, Y. Wang, X. Wang and X. Zhu, "Thiol-ene" crosslinked polybenzimidazoles anion exchange membrane with enhanced performance and durability, *J. Colloid Interface Sci.*, 2023, **638**, 349–362.

21 X. Wu, N. Chen, C. Hu, H.-A. Klok, Y. M. Lee and X. Hu, Fluorinated poly (aryl piperidinium) membranes for anion exchange membrane fuel cells, *Adv. Mater.*, 2023, **35**, 2210432.

22 X. Li, B. Zhang, J. Guo, Y. Chen, L. Dai, J. Zheng, S. Li and S. Zhang, High-strength, ultra-thin anion exchange membranes with a branched structure toward alkaline membrane fuel cells, *J. Mater. Chem. A*, 2023, **11**, 10738–10747.

23 B. Liu, T. Li, Q. Li, S. Zhu, Y. Duan, J. Li, H. Zhang and C. Zhao, Enhanced diffusion dialysis performance of cross-linked poly (aryl piperidine) anion exchange membranes by thiol-ene click chemistry for acid recovery, *J. Membr. Sci.*, 2022, **660**, 120816.

24 J. Chen, Y. S. L. Choo, X. Wang, Y. Liu, X. Yue, X. Gao, W. Gao, Q. Zhang, A. Zhu and Q. Liu, Effects of the crown ether cavity on the performance of anion exchange membranes, *J. Colloid Interface Sci.*, 2023, **643**, 62–72.

25 X. Wang, X. Qiao, S. Liu, L. Liu and N. Li, Poly (terphenyl piperidinium) containing hydrophilic crown ether units in main chains as anion exchange membranes for alkaline fuel cells and water electrolysers, *J. Membr. Sci.*, 2022, **653**, 120558.

26 W. Liu, L. Liu, J. Liao, L. Wang and N. Li, Self-crosslinking of comb-shaped polystyrene anion exchange membranes for alkaline fuel cell application, *J. Membr. Sci.*, 2017, **536**, 133–140.

27 S. Li, X. Zhu, D. Liu and F. Sun, A highly durable long side-chain polybenzimidazole anion exchange membrane for AEMFC, *J. Membr. Sci.*, 2018, **546**, 15–21.

28 Y. Yuan, X. Du, Z. Sui, S. Wang, T. Dong, X. Chi and Z. Wang, Host-guest coordination self-assembly gives anion exchange membranes better stability, *Chem. Eng. J.*, 2023, **464**, 142563.

29 F. Wang, Y. Li, C. Li and H. Zhu, Preparation and study of spirocyclic cationic side chain functionalized polybiphenyl piperidine anion exchange membrane, *J. Membr. Sci.*, 2021, **620**, 118919.
30 L. Tian, J. Li, Q. Liu, W. Ma, F. Wang, H. Zhu and Z. Wang, Cross-Linked anion-exchange membranes with dipole-containing cross-linkers based on poly (terphenyl isatin piperidinium) copolymers, *ACS Appl. Mater. Interfaces*, 2022, **14**, 39343–39353.
31 P. Sharma, M. Manohar, S. Kumar and V. K. Shahi, Highly charged and stable cross-linked polysulfone alkaline membrane for fuel cell applications: 4, 4-((3,3′-bis(chloromethyl)-(1,1′-biphenyl)-4,4-diyl)bis(oxy))dianiline (BCBD) a novel cross-linker, *Int. J. Hydrogen Energy*, 2020, **45**, 18693–18703.
32 C. G. Morandi, R. Peach, H. M. Krieg and J. Kerres, Novel imidazolium-functionalized anion-exchange polymer PBI blend membranes, *J. Membr. Sci.*, 2015, **476**, 256–263.
33 J. Xu, M. Ju, X. Chen, L. Meng, J. Ren, J. Lei, P. Zhao and Z. Wang, High alkaline stability and long-term durability of imidazole functionalized poly(ether ether ketone) by incorporating graphene oxide/metal-organic framework complex, *Int. J. Hydrogen Energy*, 2022, **47**, 25755–25768.
34 H. Han, H. Ma, J. Yu, H. Zhu and Z. Wang, Preparation and performance of novel tetraphenylphosphonium-functionalized polyphosphazene membranes for alkaline fuel cells, *Eur. Polym. J.*, 2019, **114**, 109–117.
35 H. Tang, D. Li, N. Li, Z. Zhang and Z. Zhang, Anion conductive poly (2,6-dimethyl phenylene oxide)s with clicked bulky quaternary phosphonium groups, *J. Membr. Sci.*, 2018, **558**, 9–16.
36 Z. He, G. Wang, C. Wang, L. Guo, R. Wei, G. Song, D. Pan, R. Das, N. Naik, Z. Hu and Z. Guo, Overview of anion exchange membranes based on ring opening metathesis polymerization (ROMP), *Polym. Rev.*, 2021, **61**, 689–713.
37 I. Kyungmin, C. K. Hwan, P. B. Jun, Y. S. Jong and K. Jinsoo, Tofu-derived heteroatom-doped carbon for oxygen reduction reaction in an anion exchange membrane–fuel cell, *Energy Convers. Manage.*, 2022, **265**, 115754.
38 Y. Yuan, X. Du, H. Zhang, H. Wang and Z. Wang, Poly (isatin biphenylene) polymer containing ferrocenium derivatives for anion exchange membrane fuel cell, *J. Membr. Sci.*, 2022, **642**, 119986.
39 X. Wang and R. G. H. Lammertink, Dimensionally stable multication-crosslinked poly (arylene piperidinium) membranes for water electrolysis, *J. Mater. Chem. A*, 2022, **10**, 8401–8412.
40 X. Du, Z. Wang, H. Zhang, Y. Yuan, H. Wang and Z. Zhang, Prepared poly (aryl piperidinium) anion exchange membranes for acid recovery to improve dialysis coefficients and selectivity, *J. Membr. Sci.*, 2021, **619**, 118805.
41 Q. Liu, W. Ma, L. Tian, J. Li, L. Yang, F. Wang, Z. Wang, J. Li, Z. Wang and H. Zhu, Side-chain cation-grafted poly (biphenyl piperidine) membranes for anion exchange membrane fuel cells, *J. Power Sources*, 2022, **551**, 232105.
42 Z. Zhao, M. Zhang, W. Du, Y. Xiao, Z. Yang, D. Dong, X. Zhang and M. Fan, Strong and flexible high-performance anion exchange membranes with long-distance interconnected ion transport channels for alkaline fuel cells, *ACS Appl. Mater. Interfaces*, 2022, **14**, 38132–38143.
43 T. Yu, S. Li, L. Zhang, F. Li, J. Wang, H. Pan and D. Zhang, In situ growth of ZIF-67-derived nickel-cobalt-manganese hydroxides on 2D V_2CT_x MXene for dual-functional orientation as high-performance asymmetric supercapacitor and electrochemical hydroquinone sensor, *J. Colloid Interface Sci.*, 2023, **629**, 546–558.
44 J. Zhang, K. Zhang, X. Liang, W. Yu, X. Ge, M. A. Shehzad, Z. Ge, Z. Yang, L. Wu and T. Xu, Self-aggregating cationic-chains enable alkaline stable ion-conducting channels for anion-exchange membrane fuel cells, *J. Mater. Chem. A*, 2021, **9**, 327–337.
45 T. H. Pham, J. S. Olsson and P. Jannasch, Poly(arylene alkylene)s with pendant N-spirocyclic quaternary ammonium cations for anion exchange membranes, *J. Mater. Chem. A*, 2018, **6**, 16537–16547.
46 X. Chu, S. Miao, A. Zhou, S. Liu, L. Liu and N. Li, A strategy to design quaternized poly (2,6-dimethyl-1,4-phenylene oxide) anion exchange membranes by atom transfer radical coupling, *J. Membr. Sci.*, 2022, **649**, 120397.
47 C.-M. Min, S.-B. Lee, M.-K. Ahn, J. Jang and J.-S. Lee, Preparation of polymer electrolyte membranes based on poly (phenylene oxide) with different side chain lengths of phosphonic acid, *J. Polym. Sci., Part A: Polym. Chem.*, 2019, **57**, 1180–1188.
48 P. F. Msomi, P. T. Nonjola, P. G. Ndungu and J. Ramontja, Poly (2, 6-dimethyl-1, 4-phenylene)/polysulfone anion exchange membrane blended with TiO_2 with improved water uptake for alkaline fuel cell application, *Int. J. Hydrogen Energy*, 2020, **45**, 29465–29476.
49 T. Zhao, C. Long, Z. Wang and H. Zhu, Multication cross-linked poly (p-terphenyl isatin) anion exchange membranes for fuel cells: Effect of cross-linker length on membrane performance, *ACS Appl. Energy Mater.*, 2021, **4**, 14476–14487.
50 W. Gou, W. Gao, X. Gao, Q. Zhang, A. Zhu and Q. Liu, Highly conductive fluorinated poly(biphenyl piperidinium) anion exchange membranes with robust durability, *J. Membr. Sci.*, 2022, **645**, 120200.
51 J. Li, S. Wang, F. Liu, X. Wang, H. Chen, T. Mao and Z. Wang, Poly (aryl ether ketone)/polymeric ionic liquid with anisotropic swelling behavior for anion exchange membranes, *J. Membr. Sci.*, 2019, **581**, 303–311.
52 X. Du, H. Zhang, Y. Yuan and Z. Wang, Semi-interpenetrating network anion exchange membranes based on quaternized polyvinyl alcohol/poly (diallyldimethylammonium chloride), *Green Energy Environ.*, 2021, **6**, 743–750.
53 Y. Zheng, U. Ash, R. P. Pandey, A. G. Ozioko, J. Ponce-González, M. Handl, T. Weissbach, J. R. Varcoe, S. Holdcroft, M. W. Liberatore, R. Hiesgen and D. R. Dekel, Water uptake study of anion exchange membranes, *Macromolecules*, 2018, **51**, 3264–3278.

54 R. Ren, S. Zhang, H. A. Miller, F. Vizza, J. R. Varcoe and Q. He, Facile preparation of novel cardo Poly(oxindolebiphenylylene) with pendent quaternary ammonium by superacid-catalysed polyhydroxyalkylation reaction for anion exchange membranes, *J. Membr. Sci.*, 2019, **591**, 117320.

55 Y. Chen, P. Li, C. Yuan, L. Zeng, J. Wang, B. Li and Z. Wei, Anion exchange membranes synthesized by acetalization of poly (vinyl alcohol) for fuel cells, *ACS Appl. Energy Mater.*, 2022, **5**, 7748–7757.

56 H. Wu, Q. Yang, X. Gao, Z. Zhu, Q. Sun, Q. Zhang, A. Zhu and Q. Liu, Novel crosslinked aliphatic anion exchange membranes with pendant pentafluorophenyl groups, *Electrochim. Acta*, 2019, **321**, 134634.

57 N. Chen, S. P. Kim, C. Hu, H. H. Wang, J. H. Park, H. M. Kim and Y. M. Lee, High-performance poly(fluorenyl aryl piperidinium)-based anion exchange membrane fuel cells with realistic hydrogen supply, *J. Power Sources*, 2021, **512**, 230474.

58 J. Xue, J. Zhang, X. Liu, T. Huang, H. Jiang, Y. Yin, Y. Qin and M. D. Guiver, Toward alkaline-stable anion exchange membranes in fuel cells: Cycloaliphatic quaternary ammonium-based anion conductors, *Electrochem. Energy Rev.*, 2022, **5**, 348–400.

59 Y. Wang, X. Qiao, M. Liu, L. Liu and N. Li, The effect of –NH– on quaternized polybenzimidazole anion exchange membranes for alkaline fuel cells, *J. Membr. Sci.*, 2021, **626**, 119178.

60 W. Yuan, L. Zeng, S. Jiang, C. Yuan, Q. He, J. Wang, Q. Liao and Z. Wei, High performance poly(carbazolyl aryl piperidinium) anion exchange membranes for alkaline fuel cells, *J. Membr. Sci.*, 2022, **657**, 120676.

61 Y. Wang, D. Zhang, X. Liang, M. A. Shehzad, X. Xiao, Y. Zhu, X. Ge, J. Zhang, Z. Ge, L. Wu and T. Xu, Improving fuel cell performance of an anion exchange membrane by terminal pending bis-cations on a flexible side chain, *J. Membr. Sci.*, 2020, **595**, 117483.

62 B. Shen, B. Sana and H. Pu, Multi-block poly (ether sulfone) for anion exchange membranes with long side chains densely terminated by piperidinium, *J. Membr. Sci.*, 2020, **615**, 0376–7388.

63 F. Liu, Q. Yang, X. Gao, H. Wu, Q. Zhang, A. Zhu and Q. Liu, Anion exchange membranes with dense N-spirocyclic cations as side-chain, *J. Membr. Sci.*, 2020, **595**, 0376–7388.

64 L. Liu, X. Chu, J. Liao, Y. Huang, Y. Li, Z. Ge, M. A. Hickner and N. Li, Tuning the properties of poly (2,6-dimethyl-1,4-phenylene oxide) anion exchange membranes and their performance in H_2/O_2 fuel cells, *Energy Environ. Sci.*, 2018, **11**, 435–446.

65 A. M. A. Mahmoud, A. M. M. Elsaghier, K. Otsuji and K. Miyatake, High hydroxide ion conductivity with enhanced alkaline stability of partially fluorinated and quaternized aromatic copolymers as anion exchange membranes, *Macromolecules*, 2017, **50**, 4256–4266.

66 N. Chen, C. Long, Y. Li, C. Lu and H. Zhu, Ultrastable and high ion-conducting polyelectrolyte based on six-membered N-spirocyclic ammonium for hydroxide exchange membrane fuel cell applications, *ACS Appl. Mater. Interfaces*, 2018, **10**, 15720–15732.